

# UPS: Towards Foundation Models for PDE Solving via Cross-Modal Adaptation

Junhong Shen<sup>1</sup> Tanya Marwah<sup>1</sup> Ameet Talwalkar<sup>1</sup>

## Abstract

We introduce UPS (Unified PDE Solver), an effective and data-efficient approach to solve diverse spatiotemporal PDEs defined over various domains, dimensions, and resolutions. UPS unifies different PDEs into a consistent representation space and processes diverse collections of PDE data using a unified network architecture that combines LLMs with domain-specific neural operators. We train the network via a two-stage cross-modal adaptation process, leveraging ideas of modality alignment and multi-task learning. By adapting from pretrained LLMs and exploiting text-form meta information, we are able to use considerably fewer training samples than previous methods while obtaining strong empirical results. UPS outperforms existing baselines, often by a large margin, on a wide range of 1D and 2D datasets in PDEBench, achieving state-of-the-art results on 8 of 10 tasks considered. Meanwhile, it is capable of few-shot transfer to different PDE families, coefficients, and resolutions.

## 1. Introduction

Partial Differential Equations (PDEs) play a pivotal role in modeling and understanding real-world phenomena, such as simulating fluid dynamics and heat transfer. Although there exists a rich body of classical PDE solvers (Boyd, 2001; LeVeque, 2007; Moukalled et al., 2016), these solvers often incur significant computational costs, especially for high-dimensional PDEs, motivating the development of data-driven alternatives that utilize deep neural networks.

In particular, there has been a growing interest in developing *neural operators* (Chen & Chen, 1995), which use neural networks to approximate a solution map for a PDE family (Lu et al., 2019; Li et al., 2020a). Many works focus on training better neural operators for single PDE families (Lippe et al., 2023; Hao et al., 2023; Marwah et al., 2023) and demonstrate promising results. However, these approaches come with high sample and compute complexity,

<sup>1</sup>Carnegie Mellon University. Correspondence to: Junhong Shen <junhongs@andrew.cmu.edu>.

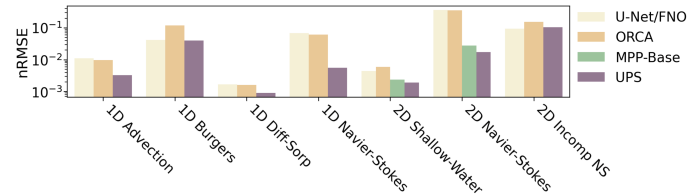


Figure 1: UPS outperforms leading competitors on a wide range of tasks from PDEBench, including the single-task neural operators U-Net (Ronneberger et al., 2015), FNO (Li et al., 2020a), and ORCA (Shen et al., 2023), and the multi-task MPP-Base (McCabe et al., 2023) (MPP only applies to 2D tasks). Here we show results for 7 in-distribution tasks, with UPS ranking first on 6 of them (details in Table 1). UPS also achieves state-of-the-art on 2 of 3 out-of-distribution tasks via few-shot transfer (details in Table 2).

since a separate model must be trained for each PDE family.

Recent works take early steps towards developing foundation models for PDE solving, aiming to learn unified models that transfer across PDE families (McCabe et al., 2023; Subramanian et al., 2023). These models are costly to develop. The network architecture must be tailored to PDEs, and the models are pretrained *from scratch* using extensive amounts of data (e.g.,  $\sim 100K$  trajectories per PDE family). Beyond computational costs, these unified models are developed solely from PDE samples; they do not leverage additional information that might be valuable for problem solving, such as the metadata (e.g., PDE names and coefficients), or more general knowledge pertaining to the entire physics domain.

We aim to develop a simple, efficient, and effective approach to learning unified neural solvers for complex time-dependent PDEs. To achieve this, rather than training from scratch as in existing efforts, we propose a novel way to adapt pretrained Large Language Models (LLMs) to PDE solving. Indeed, a burgeoning line of work has shown the capacity of LLMs in scientific fields like mathematics (Lewkowycz et al., 2022), computational biology (Vinod et al., 2023; Joachimiak et al., 2023; Shen et al., 2023), and chemistry (Bran et al., 2023; Shen et al., 2024). However, the field of PDE solving has yet to exploit large-scale models pretrained on extensive text corpora, which are capable of processing text-form information, such as metadata, and transferring to unseen tasks, even in a zero-shot fashion (Brown et al., 2020; Radford et al., 2021).

We present **Unified PDE Solver (UPS)**, which adapts pretrained LLMs to time-evolution operators for a wide range

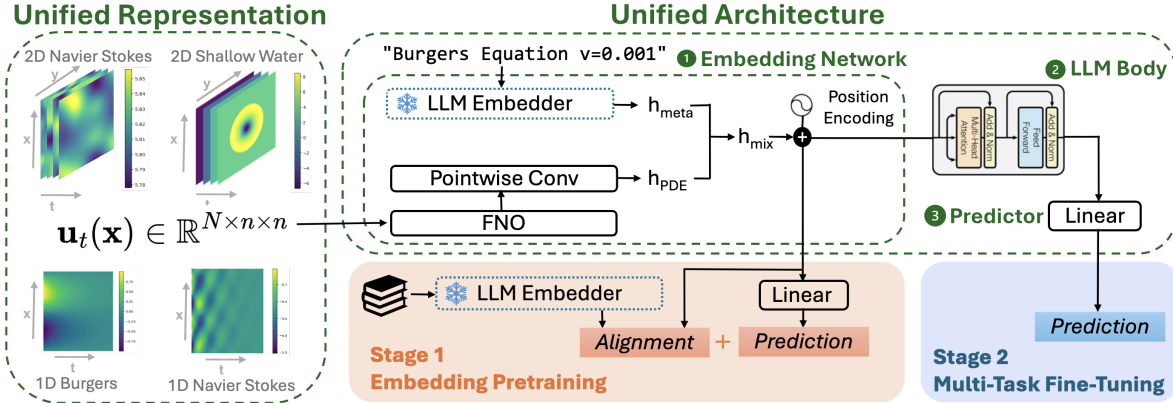


Figure 2: To adapt pretrained LLMs for PDE solving, UPS first expresses PDE trajectories of different families, dimensions, channels, and resolutions using a *unified data representation* (left panel). It then processes the data with a *unified transformer architecture* that integrates domain-specific FNO layers, PDE metadata, and LLMs for effective prediction (right panel). The architecture is trained in two stages. **In stage 1, we pretrain the embedding network** using a composite loss that simultaneously optimizes a) the distribution similarity between PDE embeddings and text embeddings to bridge the modality gap and improve alignment, and b) the prediction performance of PDE embeddings to extract useful features. **In stage 2, we fine-tune the entire model** on a dataset that combines multiple families of spatiotemporal PDEs with varying domain dimensions, initial conditions, boundary conditions, and coefficients. UPS achieves remarkable empirical results with significantly better sample-efficiency than existing methods.

of spatiotemporal PDEs (see Section 3 Equation 1 for the general form). It maps the current state of a PDE to its future state, enabling us to predict the dynamics of complex time-dependent systems. To handle PDEs of diverse families and dimensions, UPS leverages two key components.

First, we design a **unified data representation** to align different PDE trajectories into a shared feature space. Given an appropriate space and time discretization  $\mathbf{u} = \{\mathbf{u}_t(\mathbf{x})\}_{t=0}^T$ , where  $\mathbf{x} \in \mathbb{R}^d$  is the spatial variable and  $\mathbf{u}_t(\mathbf{x})$  is the state variable at time  $t$  given input  $\mathbf{x}$ , UPS takes  $\mathbf{u}_t(\mathbf{x})$  to predict  $\mathbf{u}_{t+1}(\mathbf{x})$ . Since  $\mathbf{u}_t(\mathbf{x})$  of different families may have different dimensions, we homogenize them into a shared space  $\mathbb{R}^{N \times n^{d_{\max}}}$ , where  $N$  is the number of physical quantities,  $n$  is the resolution, and  $d_{\max}$  is the maximum dimension of  $\mathbf{x}$  among all PDEs we consider.

Second, we employ a **unified network architecture** to process the unified PDE data. Inspired by a recent work, ORCA (Shen et al., 2023), which applies LLMs to diverse non-text inputs, we integrate pretrained LLMs into operator learning via a three-way architecture that consists of an embedding network, an LLM body, and a prediction network. However, different from the domain-agnostic ORCA, we design an FNO-based (Li et al., 2020a) embedding network that converts PDE data into resolution-invariant features for forward prediction. We leverage the text embeddings of the PDE metadata by combining them with the PDE features.

To effectively exploit the LLM’s pretrained knowledge and turn it into a versatile PDE solver, we propose a two-stage cross-modal adaptation process (see Figure 2 and Section 3): the embedding network is first pretrained using two objectives for modality alignment and effective prediction; then, the full model is fine-tuned on a variety of PDE datasets.

By design, UPS can handle a diverse range of PDE families, data dimensions, channels, and resolutions. It also reduces the manual effort required to develop new architectures. More crucially, by leveraging the knowledge and capacities of pretrained LLMs, UPS obtains strong performance with less training data and compute—it achieves state-of-the-art performance across a spectrum of 8 datasets from PDEBench (Takamoto et al., 2022), using fewer than 5K training trajectories for every PDE family (Figure 1). This is about  $20\times$  more sample-efficient than existing unified models. We also confirm that UPS demonstrates key properties of neural operators, such as grid- and resolution-invariance.

Beyond prediction accuracy, we show that UPS is compatible with a variety of LLM backbones, such as RoBERTa (Liu et al., 2019), T5 (Raffel et al., 2020), and CLIP (Radford et al., 2021). It also demonstrates better performance when scaled to larger backbones within the same LLM family. Hence, the model-agnostic design of UPS offers a systematic approach to leveraging the rapid advancements in LLMs for tackling PDE problems. We view UPS as a step towards building generalized foundation models for more complex physical systems in a compute-efficient manner. Code is available at <https://github.com/sjunhongshen/UnifiedPDESolvers>.

## 2. Related Work

Recent years has seen a variety of neural-network-based methods for approximating the solution of PDEs. Several works propose hybrid solvers (Hsieh et al., 2019; Bar-Sinai et al., 2019; Kochkov et al., 2021), where neural networks are used along with classical solvers like finite element/volumn methods (LeVeque, 2007; Moukalled et al.,

2016) or (pseudo)-spectral methods (Boyd, 2001; Kopriva, 2009). These works typically apply classical solvers to a low-resolution grid and use neural networks to predict the correction terms. Other works directly approximate the PDE solution with neural networks (Sirignano, 2017; Raissi et al., 2019; Khoo et al., 2021), employing variational losses (Yu et al., 2018) and physical constraints defined by the PDE (Raissi et al., 2019; Bruna et al., 2024). However, these methods are mostly equation-specific and could solve one PDE at a time. The learned models cannot be applied to other PDEs from the same family, let alone other families.

A more general approach involves learning neural operators (Lu et al., 2019; Li et al., 2020a;b), which are approximations of an infinite-dimensional operator between two functional spaces. For time-dependent PDEs, a neural operator maps the current state of a PDE to the next state, with quantities like initial conditions provided as input. Neural operators can be implemented using any architecture. For example, Fourier neural operator (FNO) (Li et al., 2020a) uses convolution-based integral kernels evaluated in the Fourier space. Other works also use transformer models (Cao, 2021; Li et al., 2022; Hao et al., 2023) or U-Net (Lippe et al., 2023). Learning neural operators enables solving an entire family of PDE and they can easily adapt to new parameterizations of a PDE without fine-tuning. However, the learned operators cannot extend to different PDE families.

To facilitate operator transfer across PDE families, two recent works develop large pretrained models for multiple physical systems (Subramanian et al., 2023; McCabe et al., 2023). In particular, Subramanian et al. (2023) train a FNO-based network on steady-state linear PDEs with periodic boundary conditions and study the model’s transfer ability when its size increases. McCabe et al. (2023) design a new transformer architecture based on the axial attention (Ho et al., 2020) and train it using various 2D non-linear, time-dependent PDEs. Their results show that a unified operator can outperform baselines trained on a single PDE family.

While our work shares a similar motivation for developing general and versatile solvers, we differ from the above work in three aspects. *Modeling-wise*, existing unified methods are limited to two-dimensional PDEs, whereas UPS tackles both one- and two-dimensional PDEs. Our training process can be also extended to any  $d$ -dimensional systems. *Architecture-wise*, these methods use PDE-specific networks and train them from scratch. However, we leverage pretrained LLMs and text-form metadata to improve downstream performance. *Efficiency-wise*, pretraining large models from scratch requires vast amount of pretraining data (e.g., 100K samples per PDE family), which can be prohibitive to collect for high-dimensional and complex PDEs. In contrast, by adapting from pretrained models and using an efficient way to close the modality gap between

text and PDE, our method requires far less fine-tuning data.

A final work that is closely related to ours is ORCA (Shen et al., 2023), which proposes a general workflow for adapting pretrained transformers to non-text, non-vision inputs. While ORCA uses PDEBench in its evaluation, it is not tailored to PDE solving and requires adapting a separate model for every PDE dataset. The resulting models are not grid- or resolution-invariant, which are key properties of neural operators for PDEs. Moreover, by learning from multiple PDEs and sharing knowledge across families, our method obtains significantly better empirical results than ORCA.

### 3. Methodology

Our goal is to build unified neural operators for spatiotemporal PDEs with varying domain dimensions, coefficients, initial and boundary conditions. These PDEs could model a range quantities that evolve over time, from vectors (e.g., velocity) to scalars (e.g., pressure and density). To do so, we propose UPS, which consists of a unified way to represent the PDE data and a LLM-based network to process them.

#### 3.1. Unified Data Representation

We model PDEs that follow the general form:

$$\begin{aligned} \frac{d\mathbf{u}(t, \mathbf{x})}{dt} &= L \left( \mathbf{u}(t, \mathbf{x}), \frac{\partial \mathbf{u}(t, \mathbf{x})}{\partial \mathbf{x}}, \frac{\partial \mathbf{u}(t, \mathbf{x})}{\partial \mathbf{x}^2}, \dots \right) \\ u(0, \mathbf{x}) &= u_0(\mathbf{x}) \\ B(\mathbf{u}(t, \mathbf{y})) &= 0 \end{aligned} \quad (1)$$

where  $\mathbf{x} \in \Omega \subset \mathbb{R}^d$  is the spatial variable,  $\mathbf{u} : [0, T] \times \Omega \rightarrow \mathbb{R}^{d_u}$  is a time-varying function defined over the domain  $\Omega$  for finite time  $T$ . Here,  $L$  is a (possibly non-linear) operator which acts on  $\mathbf{u}$  and multiple partial derivatives of  $\mathbf{u}$  w.r.t the spatial variable  $\mathbf{x}$ .  $\mathbf{u}_0(\mathbf{x}) : \Omega \rightarrow \mathbb{R}^{d_u}$  denotes the initial condition of the PDE, and the operator  $B$  defines the boundary condition where  $\mathbf{y} \in \partial\Omega$  is a point on the boundary of the domain. PDE families in this form include Navier-Stokes equations, Reaction-Diffusion equations, Burgers equations, and many others that are used to describe phenomena like fluid dynamics and heat flow over time. They also constitute most PDE benchmarks considered in machine learning (Takamoto et al., 2022; Tu et al., 2022).

Consider a set of  $S$  spatiotemporal PDEs  $\{\mathbf{u}^s\}_{s=1}^S$ . Here, each  $\mathbf{u}^s = \{\mathbf{u}_t^s(\mathbf{x})\}_{t=1}^{T_s}$  is solution to a PDE of the form defined in Equation 1 such that for all  $t \in [T_s]$ , we have  $\mathbf{u}_t^s(\mathbf{x}) \in \mathbb{R}^{d_u}$  and  $\mathbf{x} \in \Omega^s \subset \mathbb{R}^{d^s}$ . For each  $\mathbf{u}_t^s$ , we assume that we have an  $n$ -point discretization of the functions  $\{\mathbf{u}_t^s\}_{t=1}^{T_s}$  at points  $W_n^s = \{x_1^s, x_2^s, \dots, x_n^s\}$ , where each  $x_i^s \in \mathbb{R}^{d^s}$ . That is, for each PDE  $s \in S$  and  $t \in T_s$ , we have the realization of the function  $\mathbf{u}_t^s$  on a grid with each dimension divided into  $n$  parts. We assume that  $n$  is constant across PDE families. Denote the set of  $N$  physical quantities

considered for each PDE as  $V = \{v_1, v_2, \dots, v_N\}$ .

Our goal is to learn an operator  $\mathcal{G}_\theta$  which, for a given PDE  $s$ , predicts the state of the PDE at time  $t + 1$  based on its state at time  $t \in [T_s]$ . That is:

$$\mathbf{u}_{t+1}^s(\mathbf{x}) = \mathcal{G}_\theta(\mathbf{u}_t^s(\mathbf{x}))$$

Hence, we need to define a unified representation for the inputs so a model can handle all different quantities at once.

**Unifying Dimension** Let  $d = \max_{s \in S} d^s$ . We want to represent all datasets in  $\mathbb{R}^d$ . Thus, for PDEs with  $d^s < d$ , the final  $d - d^s$  coordinates of  $x_i^s \in W_n^s$  are set to zero. In this work, we mainly consider PDEs defined over one- and two-dimensional domains, i.e.,  $d^s \in \{1, 2\} \forall s \in S$ . Hence, for PDEs with  $d^s = 1$ , the point  $x \in \Omega^s$  is represented as  $(x, 0)$ . Note that our methodology to unify the total number of dimensions in the PDE is general and can be adapted to PDEs defined in higher-dimensional domains as well. In the following, we will denote  $\mathbf{u}_t^s(\mathbf{x})$  as the value of the the function  $\mathbf{u}_t^s$  on all the points in  $W_n^s$ , unless stated otherwise.

**Unifying Physical Quantities** We consider a fixed set  $V = \{v_1, v_2, \dots, v_N\}$  of  $N$  physical quantities and only train our model on the physical quantities that belong to  $V$  for each PDE. The quantities that we consider in this paper are velocity (in the  $x$  and  $y$  directions), pressure, and density, which means  $N = 4$ . If a dataset does not use a particular quantity, the entire dimension corresponding to it is set to 0.

Following the above procedure, we lift every PDE to a unified spaced such that  $\mathbf{u}^s \in \mathbb{R}^{T_s \times N \times n^d} \forall s \in S$ . To obtain the datasets for the forward prediction problem, we generate input-output pairs via autoregressive teacher-forcing: for each time step  $t \in [T_s]$ , we use  $\mathbf{u}_t^s$  to predict  $\mathbf{u}_{t+1}^s$ , thereby yielding  $T_s - 1$  pairs of data from a single trajectory. We also append the coordinates of each  $x_i^s \in W_n^s$  to the input and maintain an output mask for each data point, masking out the zero-padded dimensions when computing the loss.

### 3.2. Unified Architecture

Large-scale transformer models have demonstrated success in various application domains, spanning natural language processing (e.g., Touvron et al., 2023), computer vision (e.g., Dosovitskiy et al., 2021), and audio processing (e.g., Lu et al., 2023). In this work, we explore the potential of transformers for PDE solving. We break down the UPS architecture into three parts: an embedding network that transforms the unified representation to sequential features; the model body, representing the pretrained LLM layers; and a predictor that generates the prediction.

**FNO Embedding Network** The embedding network plays two roles. First, it projects the PDE  $\mathbf{u}_t^s(\mathbf{x})$  into the LLM’s sequential embedding space  $\mathbb{R}^{l \times e}$ , where  $l$  denotes the sequence length of the embedded features and  $e$  denotes the

LLM’s hidden dimension. Second, it should extract key features of the PDE input to enable subsequent transformer layers to make predictions. Therefore, we design a PDE-specific embedding network with FNO layers for feature extraction, a linear layer for dimensionality matching, and a concatenation operator for adding metadata (Figure 2).

We use FNO (Li et al., 2020a) due to its strong performance on various benchmarks (Takamoto et al., 2022) and its ability to extract resolution-invariant features. Since we consider maximum two-dimensional PDEs in this paper, we use a sequence of 2D FNO layers with  $l$  channels to obtain PDE features in  $\mathbb{R}^{l \times n^d}$ . To map the FNO output to the LLM’s embedding dimension, we transpose it, apply a pointwise convolution with input channel  $n^d$ , output channel  $e$ , kernel size 1, and stride 1, and transpose back. This yields the desired sequential features  $h_{\text{PDE}} \in \mathbb{R}^{l \times e}$ .

Given that UPS is intended to handle diverse data from various generating sources, we leverage the metadata related to the PDE in addition to the input dynamics. The motivation is that LLMs can use the textual information to better understand the context and specific characteristics of different PDEs. To implement this, we specify the metadata in the form “[PDE family][coefficients]” which is embedded into sequential features  $h_{\text{meta}}$  using the pretrained LLM’s tokenizer and embedding layer. We then concatenate the meta features and the PDE features so that  $h_{\text{mix}} := [h_{\text{meta}}, h_{\text{PDE}}]$ . Finally, we add positional encoding and apply layer normalization to  $h_{\text{mix}}$ . This will be the input to the subsequent transformer layers.

In Section 5.3, we perform various ablation studies on the embedding network. We investigate different hyperparameters, such as the channel dimension  $l$  for FNO, which determines the expressivity of the embedded PDE features. We also show that incorporating metadata improves both prediction performance and generalization ability of UPS.

**Utilizing Pretrained LLMs** The main body of a UPS model consists of pretrained transformer layers from an LLM. Thus, we pass  $h_{\text{mix}}$  to the pretrained transformer layers, which produce the hidden states  $\hat{h} \in \mathbb{R}^{l \times e}$ . Note that we do not apply autoregressive masking to  $h_{\text{mix}}$  and allow the embedded features to attend to each other, since there is no causal structure in the spatial dimensions of a PDE.

Our design provides flexibility for using different LLMs as the model body. We show experiment results with multiple LLMs in Section 5.3. While different LLMs have different performance, they are competitive with existing baselines. We also show that adapting from pretrained weights outperforms training the same architecture from scratch, so UPS is especially useful for low-data regimes.

**Linear Predictor** Finally, we define a prediction head to transform the hidden state of the LLM body  $\hat{h}$  to the



predicted next step of the input  $\hat{\mathbf{u}}_{t+1}^s(\mathbf{x}) \in \mathbb{R}^{N \times n^d}$  (we predict all the physical quantities in the set  $V$ ). This is achieved by averaging over the sequence dimension of  $\hat{h}$  to get shape  $\mathbb{R}^e$ , applying a linear layer to map it to  $\mathbb{R}^{Nn^d}$ , and reshaping the results to obtain the final prediction  $\hat{\mathbf{u}}_{t+1}^s(\mathbf{x})$ .

#### 4. Full Workflow and Training

We train UPS in two stages. In the first stage, we train the embedding network to align  $h_{\text{mix}}$  with the LLM’s embedding space. This is because LLMs are trained for the text modality, which has distinct characteristics and features from physical processes like fluid dynamics and heat flow. Stage 1 reduces the modality gap to prevent the distortion of pretrained weights. Next, we fine-tune the entire model on a dataset of multiple families of spatiotemporal PDEs.

**Stage 1: Embedding Pretraining** Intuitively, there is a modality gap between text data used to train general-purpose LLMs and PDEs. Previous work has also shown that directly fine-tuning pretrained LLMs on non-text inputs can result in suboptimal performance (Lu et al., 2022). To address this challenge, Shen et al. (2023) introduced ORCA, which performs distribution matching before fine-tuning to enable cross-modal adaptation. That is, given a randomly initialized embedding network, we first pretrain it to minimize the distribution distance between the embedding network’s output—in our case  $h_{\text{mix}}$ —and the distribution of the text embeddings of a reference NLP dataset, which we denote as  $h_{\text{LM}}$ . This process makes the cross-modal distribution resemble the text distribution that the LLM is pretrained on.

We apply similar alignment to the PDE features  $h_{\text{mix}}$ . However, unlike ORCA which uses an optimal transport (OT) based metric for measuring the distribution distance, we use the maximum mean discrepancy (MMD) distance for UPS. This is because the OT-based metric requires discrete class labels to compute, making it unsuitable for PDEs. In contrast, MMD acts directly on the features  $h_{\text{mix}}$  and is more computationally efficient. Thus, we define

$$\begin{aligned} \mathcal{L}_{\text{align}} &= \|\mu_{\mathcal{D}_{h_{\text{mix}}}} - \mu_{\mathcal{D}_{h_{\text{LM}}}}\|_{L_2} \\ &= \mathbb{E}_{\mathcal{D}_{h_{\text{mix}}}}[k(a, a')] - 2\mathbb{E}_{\mathcal{D}_{h_{\text{mix}}}, \mathcal{D}_{h_{\text{LM}}}}[k(a, b)] \\ &\quad - \mathbb{E}_{\mathcal{D}_{h_{\text{LM}}}}[k(b, b')] \end{aligned} \quad (2)$$

where  $k(a, a') = \exp(-\|a - a'\|_2/2)$  denotes the Gaussian kernel;  $\mathcal{D}_{h_{\text{mix}}}$  and  $\mathcal{D}_{h_{\text{LM}}}$  denote the distributions of the PDE embeddings  $h_{\text{mix}}$  and the reference text embeddings  $h_{\text{LM}}$ .

To improve the feature extraction ability of the embedding network in the context of our downstream task, we also introduce a *task loss* for PDE forward prediction, i.e., the normalized root mean squared (nRMSE) loss between the prediction  $\hat{\mathbf{u}}_{t+1}^s(\mathbf{x})$  and the ground truth  $\mathbf{u}_{t+1}^s(\mathbf{x})$ :

$$\mathcal{L}_{\text{task}} = \frac{1}{S} \sum_{s=0}^S \frac{1}{T_s} \sum_{t=0}^{T_s-1} \frac{\|\mathbf{u}_{t+1}^s(\mathbf{x}) - \hat{\mathbf{u}}_{t+1}^s(\mathbf{x})\|_2}{\|\mathbf{u}_{t+1}^s(\mathbf{x})\|_2} \quad (3)$$

Therefore, the final objective used to pretrain the embedding network consists of both the alignment loss and the task loss:  $\mathcal{L}_{\text{emb}} = \mathcal{L}_{\text{align}} + \mathcal{L}_{\text{task}}$ . We show in Section 5.3 that both objectives are essential to the overall performance of UPS.

**Stage 2: Multi-Task Fine-Tuning** In contrast to most existing neural PDE solvers, which train a separate model for each dataset, UPS is trained using one large dataset consisting of PDE data from multiple generating sources (all of  $S$ ). Hence, after learning the embedding network, we fine-tune the entire model (the embedding network, the LLM body, and the linear predictor) using  $\mathcal{L}_{\text{task}}$  defined in Equation 3. We evaluate the performance of UPS in Section 5.1 and find it outperforms existing single-dataset neural operators. We also show that UPS generalizes to unseen PDE families and coefficients (Section 5.2)—the zero-shot and few-shot adaptation performance is competitive with models specifically trained on the entire target dataset.

### 5. Experiments

**Data** We train and evaluate our method using PDEBench (Takamoto et al., 2022). For training, we combine 7 datasets from different PDE families: Burgers Equation (1D), Advection (1D), Diffusion-Sportion (1D), Shallow-Water (2D), compressible Navier-Stokes (1D and 2D), and incompressible Navier-Stokes (2D). We explicitly hold out two families—1D and 2D Diffusion-Reaction—to evaluate the generalization performance of UPS. The dataset details, sizes, and coefficients can be found in Appendix A. We use the scale-independent normalized root mean squared error (nRMSE) as the evaluation metric, defined as follows:

$$\text{nRMSE} = \frac{1}{S_{\text{test}}} \sum_{s=1}^{S_{\text{test}}} \frac{\|\mathbf{u}^s(\mathbf{x}) - \hat{\mathbf{u}}^s(\mathbf{x})\|_2}{\|\mathbf{u}^s(\mathbf{x})\|_2} \quad (4)$$

We preprocess all the PDEs by normalizing each dataset along the channel dimension to ensure that the scale of  $\mathbf{u}_t^s(\mathbf{x})$  across different datasets is similar. The model’s prediction is denormalized to compute nRMSE.

**Baselines** We compare against three sets of baselines: 1) physics-informed neural network (PINN) (Raissi et al., 2019), which fits a network *per example*; 2) single-task models trained on individual PDE datasets, including the generic image regression model U-Net (Ronneberger et al., 2015), FNO (Li et al., 2020b), and LLM-based ORCA (Shen et al., 2023); 2) a multi-task model trained on multiple datasets, MPP (McCabe et al., 2023). We note that MPP is only applicable to 2D PDEs and it is pretrained on Navier-Stokes, Shallow-Water, and Diffusion-Reaction from PDEBench. Subramanian et al. (2023) is not included as a baseline because its models are pretrained on different

Table 1: nRMSEs (lower is better) for in-distribution PDEBench families, with baseline results taken from Takamoto et al. (2022); Shen et al. (2023); McCabe et al. (2023). On 6 of 7 datasets, UPS achieves the lowest nRMSEs. ‘-’ means that the result is not available.

		# Params	Advection 1D	Burgers 1D	Diffusion-Sorption 1D	Navier-Stokes 1D	Shallow-Water 2D	Navier-Stokes 2D	Incomp Navier-Stokes 2D
Single-Example	PINN	8.5K	1.1	0.96	0.22	-	0.017	-	-
Single- Task	U-Net	7.7M	0.67	0.34	0.15	0.72	0.083	5.1	0.1903
	FNO	466K	0.011	0.042	0.0017	0.068	0.0044	0.36	<b>0.0942</b>
	ORCA (RoBERTa-Base)	125M	0.0098	0.12	0.0016	0.062	0.006	0.3549	0.1529
Multi- Task	MPP-Base	116M	-	-	-	-	0.0024	0.0281	-
	MPP-Large	409M	-	-	-	-	0.0022	0.0208	-
	UPS (RoBERTa-Base)	149M	<b>0.0033</b>	<b>0.0399</b>	<b>0.0009</b>	<b>0.0056</b>	<b>0.0019</b>	<b>0.0174</b>	0.104

PDE families (e.g., Poisson’s and Helmholtz equations) and are not trained or evaluated using PDEBench.

**Implementation Details** As noted in Section 3, UPS is compatible with any pretrained LLM. We present our main results using RoBERTa (Liu et al., 2019) and show the performance of other backbones in ablation studies (Table 4). We set the embedding FNO channel  $l$  to 32. Since the resolution of the 2D datasets in PDEBench is 128, we set the model resolution  $n$  to 128 and downsample datasets with higher resolutions. See Appendix B for training details. Note that all of our experiments can be run on a single NVIDIA A6000 GPU because we use fewer training data.

### 5.1. State-of-the-Art Results on PDEBench

We first study the *in-distribution* performance of UPS. That is, we evaluate UPS on the test splits of the datasets that are used to train UPS, which consists of PDEs that share the same boundary conditions and coefficients with the training samples, but have different initial conditions. The results are shown in Table 1. In general, UPS with RoBERTa-Base ranks first on 6 of 7 datasets and improves the state-of-the-art by an order of magnitude on most 1D datasets. Specifically, we outperform all task-specific baselines like FNO and ORCA, which train a different model for every PDE family. This shows the benefits of learning a versatile neural operator rather than multiple specialized ones. We also outperform the unified MPP on all 2D datasets (since MPP does not apply to 1D PDEs). Note that MPP-Large is trained from scratch and uses  $4\times$  more parameters.

We emphasize that UPS is trained on significantly fewer trajectories per PDE family ( $<5K$ ) compared to MPP trained on about 100K samples for some families. Thus, our method can be run on a single GPU for less time while maintaining good performance. This shows that adapting from pretrained models makes UPS data- and compute-efficient. In addition to Table 1, we also visualize the outputs of UPS in Appendix D and show that it is indeed able to capture the the key features and dynamics of different PDE families.

### 5.2. Generalization to Unseen PDEs

In this section, we investigate the generalization (*out-of-distribution*) performance of UPS under three scenarios:

Table 2: Zero- and few-shot transfer performance of UPS on unseen PDE families and coefficients. Our few-shot results are competitive with baselines trained from scratch on larger datasets.

	# Samples	Unseen PDE Families		Unseen Coefficients
		1D Diff-React	2D Diff-React	Burgers $\nu = 1.0$
UPS	0	0.0557	1.0593	0.0566
	10	0.0107	0.9982	0.0134
	50	0.0052	0.8464	0.0039
	100	0.0034	0.7532	0.0022
	500	<b>0.001</b>	0.3625	<b>0.0009</b>
U-Net	9K	0.006	0.84	0.36
FNO		0.0014	<b>0.12</b>	0.0031
PINN		0.08	1.6	0.99
ORCA		0.003	0.82	0.012

1) unseen PDE families, 2) PDEs belonging to the same families as the training data but with different coefficients, and 3) PDEs with higher-resolution grids.

**Unseen PDE Families** As mentioned earlier, we hold out the 1D/2D Diffusion-Reaction equations from developing UPS. We first directly evaluate UPS on these two tasks and report the zero-shot transfer performance. Then, we study the few-shot transfer performance by randomly sampling  $k \in \{10, 50, 100, 500\}$  trajectories from the training sets of the held-out tasks, using them to fine-tune UPS, and evaluating UPS on the test sets. The results are shown in Table 2 and Figure 3. As the number of adaptation samples increases, the prediction error decreases. Notably, the 500-shot result of UPS on 1D Diffusion-Reaction is better than all baselines trained on the full training set. That is, we use  $20\times$  fewer data to match the performance of single-task neural solvers. This makes UPS particularly useful for real-world low-resource PDE problems where data collection is costly and training models from scratch is challenging. In Table 2, we do not include MPP because it does not apply to 1D Diffusion-Reaction, and we are unsure how many training samples are used exactly for 2D Diffusion-Reaction. That said, MPP reports strong in-distribution results on 2D Diff-React: 0.0106 (MPP-Base) and 0.0098 (MPP-Large).

**Unseen Coefficients** UPS also generalizes to PDEs in the same families as the training data but with different coefficients. We verify this by adapting UPS to Burgers Equation with  $\nu = 1.0$  (the model is trained on  $\nu = 0.001$ ). The last column in Table 2 shows that while our zero-shot performance is already competitive, the performance after further adaptation is much better than all considered baselines.

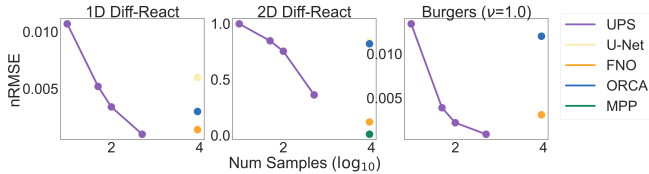


Figure 3: Visualizing UPS’s few-shot performance in Table 2.

**Unseen Resolutions** Zero-shot resolution refers to training the model on a lower resolution of the input data and evaluating them directly on a higher resolution. PDE solvers with this ability are better equipped to handle real-world scenarios where input data may vary in resolution due to practical constraints or sensor-based limitations. Recall that UPS is trained with  $n$ -point discretization  $W_n^s$ , and we set  $n = 128$  because most 2D datasets in PDEBench has resolution 128. Now, we evaluate the performance of UPS for  $n \in \{256, 512, 1024\}$ , hence increasing the resolution of the input PDE. This is achieved by downsampling the higher-resolution inputs to make them compatible with UPS and then upsampling the output prediction to the desired resolution. We do not fine-tune the model at all.

As shown in Table 3, although the nRMSEs for the Advection Equation slightly increase compared to the nRMSE for the training resolution, they still outperform all baselines in Table 1. Since the numbers are similar across columns, UPS generalizes to higher resolutions in a zero-shot manner.

### 5.3. Ablation Studies

In this section, we perform six ablation studies to understand the effects of various design decisions in UPS. S1-S5 demonstrate why adapting from pretrained LLMs is beneficial, while S6 is related to the FNO embedding network.

**S1: Pretrained LLMs vs. Training From Scratch** Compared to existing single-task models like FNO, UPS uses a transformer-based architecture with more parameters and reuses the pretrained LLM weights for the model body. To show that our results are not solely attributed to the model size and that cross-modal adaptation is important, we evaluate the model’s performance when we do *not* load the pretrained weights for the model body. This is equivalent to training a transformer model from scratch using multiple PDE datasets. As shown in Table 4, training from scratch results in worse performance than UPS, indicating the benefits of adapting and utilizing a pretrained LLM. Additionally, we find that the results of training from scratch are still better than previous single-task models like FNO and U-Net. This shows the efficacy of our overall architecture and the benefit of training a multi-tasking solver.

**S2: Cross-Modal Alignment** We also test the importance of the two objectives used in stage 1, i.e., alignment loss

Table 3: UPS is trained with resolution 128 and has an nRMSE of 0.0033 for this resolution. We directly test it on higher resolutions.

Test Resolution	256	512	1024
Advection nRMSE	0.0057	0.0064	0.0068

with MMD, and task loss with nRMSE. We study three settings: 1) using only  $\mathcal{L}_{\text{align}}$  for stage 1; 2) using only  $\mathcal{L}_{\text{task}}$  for stage 1; and 3) removing stage 1 from our workflow entirely. As shown in Table 4, while removing any objective reduces the performance across all datasets, removing the task loss has a more significant negative effect. Meanwhile, removing the entire stage of embedding pretraining hurts the prediction accuracy. This shows that simply fine-tuning the LLM without considering the modality gap or learning to extract PDE features is ineffective.

**S3: Incorporating Text-Form Metadata** UPS leverages the PDE’s metadata by combining its text embeddings with the learned PDE embeddings in the embedding network. To study whether incorporating metadata is helpful and identify an optimal approach, we compare our workflow with two alternatives: 1) we do not use metadata, so  $h_{\text{mix}} := h_{\text{PDE}}$ ; 2) we use metadata, but instead of concatenating features from two modalities, we apply a cross-attention mechanism:  $h_{\text{mix}} := \text{softmax}(\frac{QK^T}{\sqrt{e}})V$ , where  $Q = W_Q h_{\text{PDE}}$ ,  $K = W_K h_{\text{meta}}$ , and  $V = W_V h_{\text{meta}}$ . The results are shown in Table 4. UPS outperforms the non-metadata baseline, demonstrating the effect of incorporating metadata as a textual form of domain knowledge, which LLMs are able to understand. The results also suggest that feature concatenation performs better than cross-modal attention. This might be due to optimization difficulties, so we consider studying the optimal combination of metadata and PDE data as an important future direction.

**S4: Scaling LLM Backbone** In all of our results reported so far, we use RoBERTa-Base (149M parameters) as the model backbone. This allows us to study the scaling behavior of our method on various LLM sizes—we adapt UPS from RoBERTa-Large (387M parameters) and report the results in Table 4. The larger model outperforms the smaller one on all tasks, demonstrating that scaling up the backbone has the potential to yield better results. This is why we aim to adapt LLMs for PDE solving: as more resources are devoted to developing better and larger LLMs, we can potentially leverage these advancements to solve a wider range of problems in a cost-effective way.

**S5: Other LLMs/VLMs** To study whether UPS applies to other pretrained models, we further investigate Flan-T5 (Chung et al., 2022) and the vision language model CLIP (Radford et al., 2021). In particular, for CLIP, we use its text model to encode the metadata and its vision model

Table 4: Results for the ablation studies. For each set of experiments, only the specified settings are different; all the other hyperparameters and training configurations are the same. Overall, our full workflow (first row for every study) most effectively leverages the pretrained knowledge of LLMs and obtains the best empirical performance.

Study No.	Settings	Advection 1D	Burgers 1D	Diffusion-Sorption 1D	Navier-Stokes 1D	Shallow-Water 2D	Navier-Stokes 2D	Incomp Navier-Stokes 2D
S1	Pretrained LLM	<b>0.0033</b>	<b>0.0399</b>	<b>0.0009</b>	<b>0.0056</b>	<b>0.0019</b>	<b>0.0174</b>	<b>0.104</b>
	Training From Scratch	0.0055	0.0417	0.0019	0.0061	0.0022	0.0189	0.12
S2	Align and Task	<b>0.0033</b>	0.0399	<b>0.0009</b>	<b>0.0056</b>	<b>0.0019</b>	<b>0.0174</b>	<b>0.104</b>
	Task Only	0.0048	<b>0.0389</b>	<b>0.0009</b>	0.0065	0.002	0.0184	0.1046
	Align Only	0.0039	0.043	0.0011	0.0063	0.0022	0.0187	0.1092
	No Embedding Pretraining	0.0049	0.0436	0.0019	0.0072	0.0024	0.0197	0.1079
S3	Concatenation	0.0033	<b>0.0399</b>	<b>0.0009</b>	<b>0.0056</b>	<b>0.0019</b>	<b>0.0174</b>	<b>0.104</b>
	Cross-Attention	<b>0.003</b>	0.0420	<b>0.0009</b>	0.0065	0.0023	0.0189	0.1082
	No Metadata	0.0122	0.0453	0.001	0.0091	0.0026	0.0238	0.1171
S4	RoBERTa-Base	0.0033	0.0399	<b>0.0009</b>	0.0056	0.0019	0.0174	0.104
	RoBERTa-Large	<b>0.0026</b>	<b>0.0379</b>	<b>0.0009</b>	<b>0.0053</b>	<b>0.0017</b>	<b>0.016</b>	<b>0.0994</b>
S5	RoBERTa-Base	<b>0.0033</b>	0.0399	<b>0.0009</b>	<b>0.0056</b>	<b>0.0019</b>	0.0174	0.104
	Flan-T5-Base	0.0094	0.0404	0.0076	0.0098	0.0028	0.037	0.1166
	CLIP-Base	0.0046	<b>0.0321</b>	0.0018	0.0063	0.0021	<b>0.0169</b>	<b>0.1035</b>
S6	$l = 32$	0.0033	<b>0.0399</b>	<b>0.0009</b>	<b>0.0056</b>	<b>0.0019</b>	0.0174	<b>0.104</b>
	$l = 20$	<b>0.0024</b>	0.0423	<b>0.0009</b>	0.0068	0.0022	<b>0.0157</b>	0.1043
	$l = 8$	0.0032	0.0429	<b>0.0009</b>	0.0071	0.0024	0.0195	0.1064

to process the PDE data. The results are reported in Table 4. Since these models are trained using the same datasets and optimizer configuration as RoBERTa, the results are not fully optimized. Nonetheless, their performance is competitive with existing baselines, and CLIP further outperforms RoBERTa on 3 tasks. This shows the compatibility of UPS with diverse pretrained backbones. A promising direction is to study whether optimizing the training hyperparameters for each pretrained model—especially VLMs like CLIP that are trained for an additional vision modality—or increasing the amount of training samples and time according to the model size improves downstream performance.

**S6: FNO Embedder & Target Sequence Length** As discussed in Section 3, the channel  $l$  of the FNO layers in the embedding network determines the sequence length of the PDE features that will be fed into the transformer layers. To study how this hyperparameter affects learning outcomes, we vary  $l \in \{8, 20, 32\}$  and report the results in Table 4. We also visualize the test losses for all datasets in Figure 4. In general, increasing  $l$  improves the size and capacity of the embedding network, as well as the expressivity of the PDE features. This leads to lower prediction error. However, using too many parameters for the embedding network may result in a trade-off between effectiveness and efficiency.

## 6. Conclusion and Future Work

In this paper, we present UPS, a method for adapting pretrained LLMs to unified time-evolution operators that predict the next state of a PDE from the current state. UPS applies to a diverse set of PDE families defined over one- and two-dimensional domains, with varying initial conditions, boundary conditions, coefficients, and resolutions. To train

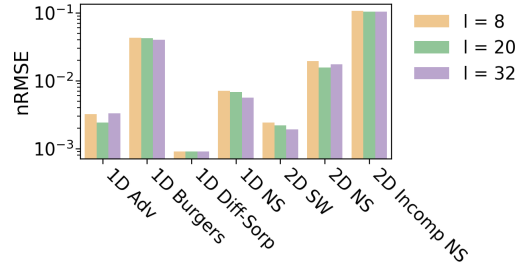


Figure 4: Varying sequence length of  $h_{\text{PDE}}$ . Longer sequence length improves the expressivity of the PDE features, leading to better performance. See Table 4 S6 for detailed numbers.

UPS, we develop a two-stage cross-modal adaptation protocol that first pretrains a FNO-based embedding network and aligns its hidden representations with the LLM’s embedding space, and then fine-tunes the entire model on a dataset containing diverse families of PDEs. Since UPS is adapted from pretrained models, it requires fewer training samples and compute than previous approaches for training unified PDE solvers from scratch. We show that UPS achieves state-of-the-art performance across multiple datasets from PDEBench and is capable of zero- and few-shot transfer to different PDE families, coefficients, and resolutions.

We identify several future directions based on our work. First, we can validate our method on a broader range of PDEs with higher-order temporal derivatives or 3-dimensional domains. Meanwhile, to seek a truly general foundation model for PDE, we aim to extend the types of tasks that UPS can solve. Currently, UPS is only applicable to forward prediction. It is important to study inverse problems of parameter estimation for different PDEs as well.



---

## 7. Broader Impact

This paper calls for ML community’s attention to take advantage of LLMs and apply them to a wider range of real-world problems beyond the NLP domains. This moves towards truly democratizing machine learning in real life. In terms of broader societal impact, our work can exert a positive influence as it contributes to reusing existing models and resources, reducing the computational burden of developing new large-scale models on massive data. However, lowering the barrier for applying LLMs to a wide range of tasks necessarily comes with the risk of misuse. Hence, it is imperative to develop adaptation methods with better privacy, safety, and fairness guarantees.

## Acknowledgement

We thank Mikhail Khodak and Wenduo Cheng for providing useful feedback on the paper. This work was supported in part by the National Science Foundation grants IIS1705121, IIS1838017, IIS2046613, IIS2112471, and funding from Meta, Morgan Stanley, Amazon, and Google. Any opinions, findings and conclusions or recommendations expressed in this material are those of the author(s) and do not necessarily reflect the views of any of these funding agencies.

## References

- Bar-Sinai, Y., Hoyer, S., Hickey, J., and Brenner, M. P. Learning data-driven discretizations for partial differential equations. *Proceedings of the National Academy of Sciences*, 116(31):15344–15349, 2019.
- Boyd, J. P. *Chebyshev and Fourier spectral methods*. Courier Corporation, 2001.
- Bran, A. M., Cox, S., White, A. D., and Schwaller, P. Chemcrow: Augmenting large-language models with chemistry tools. *arXiv preprint arXiv:2304.05376*, 2023.
- Brown, T., Mann, B., Ryder, N., Subbiah, M., Kaplan, J. D., Dhariwal, P., Neelakantan, A., Shyam, P., Sastry, G., Askell, A., et al. Language models are few-shot learners. *Advances in neural information processing systems*, 33: 1877–1901, 2020.
- Bruna, J., Peherstorfer, B., and Vanden-Eijnden, E. Neural galerkin schemes with active learning for high-dimensional evolution equations. *Journal of Computational Physics*, 496:112588, 2024.
- Cao, S. Choose a transformer: Fourier or galerkin. *Advances in neural information processing systems*, 34: 24924–24940, 2021.
- Chen, T. and Chen, H. Universal approximation to nonlinear operators by neural networks with arbitrary activation functions and its application to dynamical systems. *IEEE Transactions on Neural Networks*, 6(4):911–917, 1995.
- Chung, H. W., Hou, L., Longpre, S., Zoph, B., Tay, Y., Fedus, W., Li, Y., Wang, X., Dehghani, M., Brahma, S., Webson, A., Gu, S. S., Dai, Z., Suzgun, M., Chen, X., Chowdhery, A., Castro-Ros, A., Pellat, M., Robinson, K., Valter, D., Narang, S., Mishra, G., Yu, A., Zhao, V., Huang, Y., Dai, A., Yu, H., Petrov, S., Chi, E. H., Dean, J., Devlin, J., Roberts, A., Zhou, D., Le, Q. V., and Wei, J. Scaling instruction-finetuned language models, 2022.
- Dosovitskiy, A., Beyer, L., Kolesnikov, A., Weissenborn, D., Zhai, X., Unterthiner, T., Dehghani, M., Minderer, M., Heigold, G., Gelly, S., Uszkoreit, J., and Houshy, N. An image is worth 16x16 words: Transformers for image recognition at scale. *International Conference on Learning Representations*, 2021.
- Hao, Z., Wang, Z., Su, H., Ying, C., Dong, Y., Liu, S., Cheng, Z., Song, J., and Zhu, J. Gnot: A general neural operator transformer for operator learning. In *International Conference on Machine Learning*, pp. 12556–12569. PMLR, 2023.
- Ho, J., Kalchbrenner, N., Weissenborn, D., and Salimans, T. Axial attention in multidimensional transformers. *International Conference on Learning Representations*, 2020.
- Hsieh, J.-T., Zhao, S., Eismann, S., Mirabella, L., and Ermon, S. Learning neural pde solvers with convergence guarantees. *arXiv preprint arXiv:1906.01200*, 2019.
- Joachimiak, M. P., Caufield, J. H., Harris, N. L., Kim, H., and Mungall, C. J. Gene set summarization using large language models. *ArXiv*, 2023.
- Khoo, Y., Lu, J., and Ying, L. Solving parametric pde problems with artificial neural networks. *European Journal of Applied Mathematics*, 32(3):421–435, 2021.
- Kochkov, D., Smith, J. A., Alieva, A., Wang, Q., Brenner, M. P., and Hoyer, S. Machine learning–accelerated computational fluid dynamics. *Proceedings of the National Academy of Sciences*, 118(21):e2101784118, 2021.
- Kopriva, D. A. *Implementing spectral methods for partial differential equations: Algorithms for scientists and engineers*. Springer Science & Business Media, 2009.
- LeVeque, R. J. *Finite difference methods for ordinary and partial differential equations: steady-state and time-dependent problems*. SIAM, 2007.
- Lewkowycz, A., Andreassen, A., Dohan, D., Dyer, E., Michalewski, H., Ramasesh, V., Slone, A., Anil, C., Schlag, I., Gutman-Solo, T., et al. Solving quantitative reasoning problems with language models. *Advances in*

- Neural Information Processing Systems*, 35:3843–3857, 2022.
- Li, Z., Kovachki, N., Azizzadenesheli, K., Liu, B., Bhattacharya, K., Stuart, A., and Anandkumar, A. Fourier neural operator for parametric partial differential equations. *arXiv preprint arXiv:2010.08895*, 2020a.
- Li, Z., Kovachki, N., Azizzadenesheli, K., Liu, B., Bhattacharya, K., Stuart, A., and Anandkumar, A. Neural operator: Graph kernel network for partial differential equations. *arXiv preprint arXiv:2003.03485*, 2020b.
- Li, Z., Meidani, K., and Farimani, A. B. Transformer for partial differential equations’ operator learning. *arXiv preprint arXiv:2205.13671*, 2022.
- Lippe, P., Veeling, B. S., Perdikaris, P., Turner, R. E., and Brandstetter, J. Pde-refiner: Achieving accurate long rollouts with neural pde solvers. *arXiv preprint arXiv:2308.05732*, 2023.
- Liu, Y., Ott, M., Goyal, N., Du, J., Joshi, M., Chen, D., Levy, O., Lewis, M., Zettlemoyer, L., and Stoyanov, V. Roberta: A robustly optimized bert pretraining approach. *arXiv preprint arXiv:1907.11692*, 2019.
- Lu, J., Clark, C., Lee, S., Zhang, Z., Khosla, S., Marten, R., Hoiem, D., and Kembhavi, A. Unified-io 2: Scaling autoregressive multimodal models with vision, language, audio, and action. *ArXiv*, abs/2312.17172, 2023. URL <https://api.semanticscholar.org/CorpusID:266573555>.
- Lu, K., Grover, A., Abbeel, P., and Mordatch, I. Frozen pretrained transformers as universal computation engines. *Proceedings of the AAAI Conference on Artificial Intelligence*, 36(7):7628–7636, Jun. 2022.
- Lu, L., Jin, P., and Karniadakis, G. E. Deeponet: Learning nonlinear operators for identifying differential equations based on the universal approximation theorem of operators. *arXiv preprint arXiv:1910.03193*, 2019.
- Marwah, T., Pokle, A., Kolter, J. Z., Lipton, Z. C., Lu, J., and Risteski, A. Deep equilibrium based neural operators for steady-state pdes. *arXiv preprint arXiv:2312.00234*, 2023.
- McCabe, M., Blancard, B. R.-S., Parker, L. H., Ohana, R., Cranmer, M., Bietti, A., Eickenberg, M., Golkar, S., Krawezik, G., Lanusse, F., et al. Multiple physics pre-training for physical surrogate models. *arXiv preprint arXiv:2310.02994*, 2023.
- Moukalled, F., Mangani, L., Darwish, M., Moukalled, F., Mangani, L., and Darwish, M. *The finite volume method*. Springer, 2016.
- Radford, A., Kim, J. W., Hallacy, C., Ramesh, A., Goh, G., Agarwal, S., Sastry, G., Askell, A., Mishkin, P., Clark, J., et al. Learning transferable visual models from natural language supervision. In *International conference on machine learning*, pp. 8748–8763. PMLR, 2021.
- Raffel, C., Shazeer, N., Roberts, A., Lee, K., Narang, S., Matena, M., Zhou, Y., Li, W., and Liu, P. J. Exploring the limits of transfer learning with a unified text-to-text transformer. *The Journal of Machine Learning Research*, 21(1):5485–5551, 2020.
- Raissi, M., Perdikaris, P., and Karniadakis, G. E. Physics-informed neural networks: A deep learning framework for solving forward and inverse problems involving nonlinear partial differential equations. *Journal of Computational physics*, 378:686–707, 2019.
- Ronneberger, O., Fischer, P., and Brox, T. U-net: Convolutional networks for biomedical image segmentation. *ArXiv*, abs/1505.04597, 2015. URL <https://api.semanticscholar.org/CorpusID:3719281>.
- Sang, E. T. K. and Meulder, F. D. Introduction to the conll-2003 shared task: Language-independent named entity recognition. In *Conference on Computational Natural Language Learning*, 2003. URL <https://api.semanticscholar.org/CorpusID:2470716>.
- Shen, J., Li, L., Dery, L. M., Staten, C., Khodak, M., Neubig, G., and Talwalkar, A. Cross-modal fine-tuning: Align then refine. *arXiv preprint arXiv:2302.05738*, 2023.
- Shen, J., Tenenholtz, N., Hall, J. B., Alvarez-Melis, D., and Fusi, N. Tag-llm: Repurposing general-purpose llms for specialized domains, 2024.
- Sirignano, J and, K. S. A deep learning algorithm for solving partial differential equations. *ArXiv e-prints*, 2017.
- Subramanian, S., Harrington, P., Keutzer, K., Bhimji, W., Morozov, D., Mahoney, M., and Gholami, A. Towards foundation models for scientific machine learning: Characterizing scaling and transfer behavior. *arXiv preprint arXiv:2306.00258*, 2023.
- Takamoto, M., Praditia, T., Leiteritz, R., MacKinlay, D., Alesiani, F., Pflüger, D., and Niepert, M. Pdebench: An extensive benchmark for scientific machine learning. *Advances in Neural Information Processing Systems*, 35: 1596–1611, 2022.
- Touvron, H., Lavril, T., Izacard, G., Martinet, X., Lachaux, M.-A., Lacroix, T., Rozière, B., Goyal, N., Hambro, E., Azhar, F., Rodriguez, A., Joulin, A., Grave, E., and Lample, G. Llama: Open and efficient foundation language models. *ArXiv*, abs/2302.13971, 2023. URL <https://api.semanticscholar.org/CorpusID:257219404>.

---

Tu, R., Roberts, N., Khodak, M., Shen, J., Sala, F., and Talwalkar, A. NAS-bench-360: Benchmarking neural architecture search on diverse tasks. In *Advances in Neural Information Processing Systems (NeurIPS) Datasets and Benchmarks Track*, 2022.

Vinod, R., Chen, P.-Y., and Das, P. Reprogramming pre-trained language models for protein sequence representation learning. *arXiv preprint arXiv:2301.02120*, 2023.

Yu, B. et al. The deep ritz method: a deep learning-based numerical algorithm for solving variational problems. *Communications in Mathematics and Statistics*, 6(1):1–12, 2018.

---

## Appendix

### A. Datasets

As mentioned in Section 5, we train our models using the datasets provided in the PDEBench (Takamoto et al., 2022). The time-dependent PDE families considered by our models are: Burgers Equation (1D), Diffusion-Sorption (1D), Shallow-Water (2D), compressible Navier-Stokes (1D and 2D), incompressible Navier-Stokes (2D), and Diffusion-Reaction (1D and 2D). For each  $s \in S$ , the number of points in the  $n$ -point discretization  $W_n^s$  is 128, i.e,  $n = 128$ . For PDEs where the PDEbench-provided grid has more than 128 points in each dimension, we sample 128 equispaced points.

In this section, we provide few key properties and considerations for the PDEs used in this paper. The initial conditions  $u(0, x)$  for most of the datasets are sampled from a superposition of sinusoidal waves. The set of coefficients and number of trajectories used per PDE are reported in Appendix Table 5. For full details on the data generation process and the hyperparameters used to generate the PDE dataset, we refer the reader to Takamoto et al. (2022).

#### A.1. Burgers Equation (1D)

Burgers equation is commonly used to model the nonlinear dynamics of various fluid dynamics systems. Given the field  $u(t, x) \in (0, 2] \times (0, 1) \rightarrow \mathbb{R}$  the PDE is defined as follows:

$$\partial_t u(t, x) + \partial_x \frac{u^2(t, x)}{2} = \frac{\nu}{\pi} \partial_{xx} u(t, x) \quad (5)$$

Here  $\nu$  is the diffusion coefficient or the viscosity of the liquid, and  $\pi$  is the density of the liquid.

#### A.2. Diffusion-Sorption Equation (1D)

Diffusion-Sorption is a nonlinear diffusive process slowed down by an external force that is dependent of the state variable  $u$ . This PDE is used to model groundwater contamination transport processes. The PDE is defined as the following:

$$\partial_t u(t, x) = \frac{D}{R(u)} \partial_{xx} u(t, x), \quad (6)$$

where  $x \in (0, 1)$ ,  $t \in (0, 500]$ , and  $D = 5 \times 10^{-4}$ . For more details on the initial conditions, boundary conditions and the function  $R(u)$ , we refer the reader to Takamoto et al. (2022). For our training, we use 4500 trajectories for this PDE generated by varying the initial conditions.

#### A.3. Advection Equation (1D)

Given advection speed  $\beta$ , the advection equations are expressed as:

$$\begin{aligned} \partial_t u(t, x) + \beta \partial_x u(t, x) &= 0 \\ u(0, x) &= u_0(x) \end{aligned} \quad (7)$$

where  $x \in (0, 1)$  and  $t \in (0, 2]$ . Various examples in this dataset are generated by sampling multiple initial conditions from a super-position of sinusoidal waves as used in Takamoto et al. (2022).

#### A.4. Compressible Navier-Stokes (1D and 2D)

Given density  $\rho$ , velocity  $\mathbf{u}$ , pressure  $p$ , internal energy of the system  $\epsilon$  the compressible Navier-Stokes equations are defined as follows.

$$\begin{aligned} \partial_t p + \nabla \cdot (\rho \mathbf{u}) &= 0, \\ \rho (\partial_t \mathbf{u} + \mathbf{u} \cdot \nabla \mathbf{u}) &= -\nabla p + \eta \Delta \mathbf{u} + \left( \xi + \frac{\eta}{3} \right) \nabla (\nabla \cdot \mathbf{u}) \\ \partial_t \left( \epsilon + \rho \frac{\|\mathbf{u}\|_2^2}{2} \right) + \nabla \cdot \left( \left( p + \epsilon + \rho \frac{\mathbf{u}^2}{2} \right) \mathbf{u} - \mathbf{u} \cdot \sigma' \right) &= 0 \end{aligned} \quad (8)$$

Here,  $x \in (-1, 1)$  for 1D Navier-Stokes and  $x \in (0, 1)^2$  for 2D Navier-Stokes, and  $t \in (0, 1)$ . Compressible Navier-Stokes are used to model multiple real-world phenomena in aerodynamics and fluid dynamics.



---

### A.5. Incompressible fluid Navier-Stokes (2D)

We define the equations for incompressible fluid Navier-Stokes where we impose the condition that the fluid is “incompressible.” That is, the equation follows the following condition:

$$\nabla \cdot \mathbf{u} = 0 \quad (9)$$

For density  $\rho$  and pressure  $p$ , the equations used to generate the data in Takamoto et al. (2022) are as follows:

$$\rho(\partial_t \mathbf{u} + \mathbf{u} \cdot \nabla \mathbf{u}) = -\nabla p \mathbf{u} + \eta \Delta \mathbf{u} + \mathbf{f} \quad (10)$$

where  $\mathbf{f}$  is an external forcing function, and Dirichlet boundary conditions. Here  $x \in [0, 1]^2$  and the initial conditions  $\mathbf{u}$  and the forcing term  $\mathbf{f}$  are sampled from two-dimensional Gaussian random fields. Please refer to Takamoto et al. (2022) for more details on the data generation process.

### A.6. Reaction Diffusion (1D and 2D)

Reaction Diffusion are diffusive processes with external force applied to the system that may or may not depend over the field variable  $\mathbf{u}$ . They are often used to model many thermodynamical systems.

1D reaction diffusion is defined as follows:

$$\partial_t u(t, x) - \nu \partial_{xx} u(t, x) = \rho u(t, x)(1 - u(t, x)) \quad (11)$$

for all  $x \in (0, 1)$  and  $t \in (0, 1]$ .

For 2D reaction diffusion, let  $\mathbf{u}(t, x) = [u_1(t, x), u_2(t, x)]$ . Then the equations are defined as:

$$\begin{aligned} \partial_t u_1(t, x) &= \nu_1 \partial_{x_1 x_1} u_1 + \nu_1 \partial_{x_2 x_2} u_1 + u_1 - u_1^3 - k - u_2 \\ \partial_t u_2(t, x) &= \nu_2 \partial_{x_1 x_1} u_2 + \nu_2 \partial_{x_2 x_2} u_2 + u_2 - u_2 \end{aligned} \quad (12)$$

where  $k = 5 \times 10^{-3}$  and  $\nu_1$  and  $\nu_2$  are diffusion coefficients. Here  $x_1 \in (-1, 1)$  and  $x_2 \in (-1, 1)$  and the initial conditions are sampled from a Gaussian random field.

### A.7. Shallow-Water Equations (2D)

These are derived from Navier-Stokes and are a framework for modelling free-surface flow problems. We denote by  $u_1(x)$ , and  $u_2(x)$  as the velocities in the horizontal and vertical directions and  $h$  as the height of the water and  $b$  defining the spatially varying bathymetry (the measurement of the depth of water in oceans, rivers, or lakes). The shallow-water equations are defined as follows:

$$\begin{aligned} \partial_t h + \partial_{x_1} h u_1 + \partial_{x_2} h u_2 &= 0, \\ \partial_t h u_1 + \partial_{x_1} \left( u_1^2 h + \frac{1}{2} g_r h^2 \right) &= -g_r h \partial_{x_1} b, \\ \partial_t h u_2 + \partial_{x_2} \left( u_2^2 h + \frac{1}{2} g_r h^2 \right) &= -g_r h \partial_{x_2} b, \end{aligned} \quad (13)$$

where  $x \in [-2.5, 2.5]^2$  and  $g_r$  is the gravitational acceleration.

### A.8. Summary

The following table summarizes the coefficients of the datasets used to train and test our model (note that 1D/2D Diffusion-Reaction only appear in the test set but not the training set). We also provide the number of training and test trajectories. We generate the input-output pairs using autoregressive teacher-forcing.

## B. Training Details

### B.1. Hyperparameters

We use the following training hyperparameters for all of our experiments, unless otherwise specified. Due to time constraint, we have not performed exhaustive hyperparameter search or tailor the hyperparameters to each experiment setting.

Table 5: For each PDE family, we select one set of coefficients and use the data for training and testing UPS.

Dimension	Dataset	Coefficients	Num Train Trajectories	Num Test Trajectories	Timesteps	Resolution
1D	Advection	$\beta = 0.4$	4500	1000	41	128
	Burgers	$\nu = 0.001$	4500	1000	41	128
	Diffusion-Reaction	$\nu = 0.5, \rho = 1.0$	4500	1000	21	128
	Diffusion-Sorption	-	4050	100	21	128
	Compressible Navier-Stokes	$\eta = \zeta = 0.1, \text{rand\_periodic}$	4500	1000	21	128
2D	Shallow-Water	-	405	10	101	128
	Diffusion-Reaction	-	405	10	101	128
	Compressible Navier-Stokes	$M = \eta = \zeta = 0.1, \text{periodic}$	4500	1000	21	128
	Incompressible Navier-Stokes	$M = 0.1, \eta = \zeta = 1E - 8$	4500	1000	21	128

- Batch size: 32
- Gradient accumulation: 1
- Gradient clipping: -1
- Dropout: 0
- Optimizer: Adam
- Learning rate: 5E-5
- Weight decay: 1E-5
- Stage 1 epoch: 20
- Stage 2 epoch: 100

We use the CoNLL-2003 dataset (Sang & Meulder, 2003) as the reference dataset for alignment in stage 1.

## B.2. Compute

We run all of our experiments on a single NVIDIA A6000. Below are the detailed model size, per epoch training time (in seconds), and total training time (in hours). Note that we train the models for 100 epochs.

Table 6: Trainable parameters and training time for each LLM backbone.

	RoBERTa-Base	RoBERTa-Large	Flan-T5-Base	CLIP-Base
Num Params	149M	387M	176M	132M
Per Epoch (s)	3200	7600	3500	3000
Total (hrs)	88	211	97	83

---

## C. Detailed Experiment Results

### C.1. Few-Shot Adaptation

Compared to full fine-tuning of stage 2, we lower the learning rate when performing few-shot adaptation to prevent catastrophic forgetting.

- Batch size: 32
- Gradient accumulation: 1
- Gradient clipping: -1
- Dropout: 0
- Optimizer: Adam
- Learning rate: 1E-5
- Weight decay: 1E-5
- Epoch: 100

The following table reports the time required for few-shot experiments. Note that for Burgers equation, we train the model using  $\nu = 0.001$ , but the results here are for  $\nu = 1.0$ .

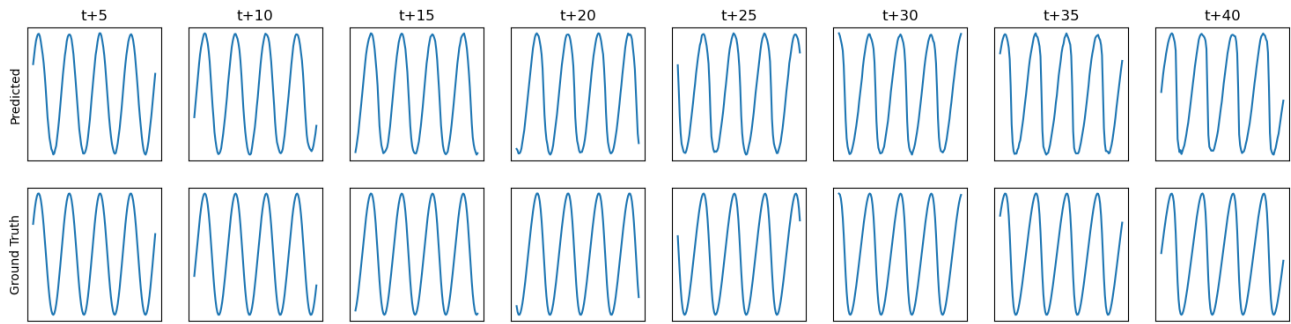
Table 7: Time for few-shot experiments. Our model outperforms most existing baselines on these tasks by using fewer than 500 samples and much shorter adaptation time.

Num Samples	1D Diffusion-Reaction		2D Diffusion-Reaction		Burgers $\nu = 1.0$	
	Per Epoch (s)	Total (hrs)	Per Epoch (s)	Total (hrs)	Per Epoch (s)	Total (hrs)
10	2	0.05	12	0.33	3	0.08
50	10	0.28	48	1.33	10	0.28
100	23	0.64	112	3.11	40	1.11
500	112	3.11	512	14.22	96	2.67

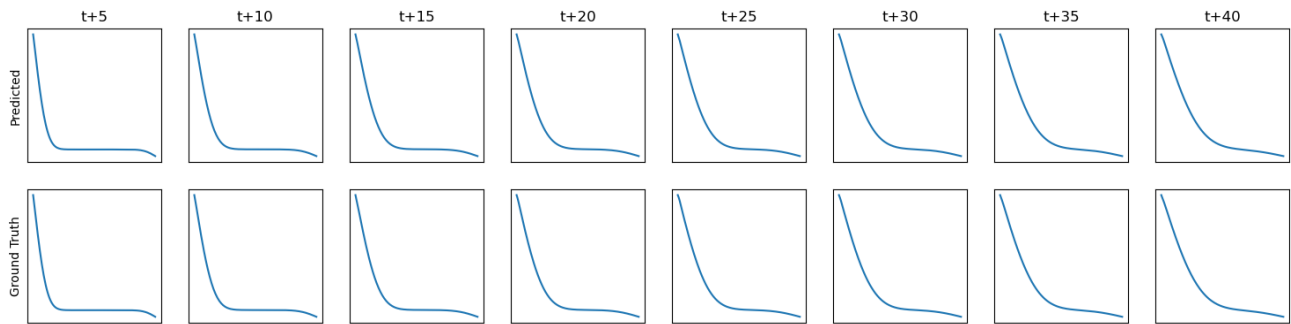
---

## D. Visualization

### D.1. Burgers Equation



### D.2. Diffusion-Sorption

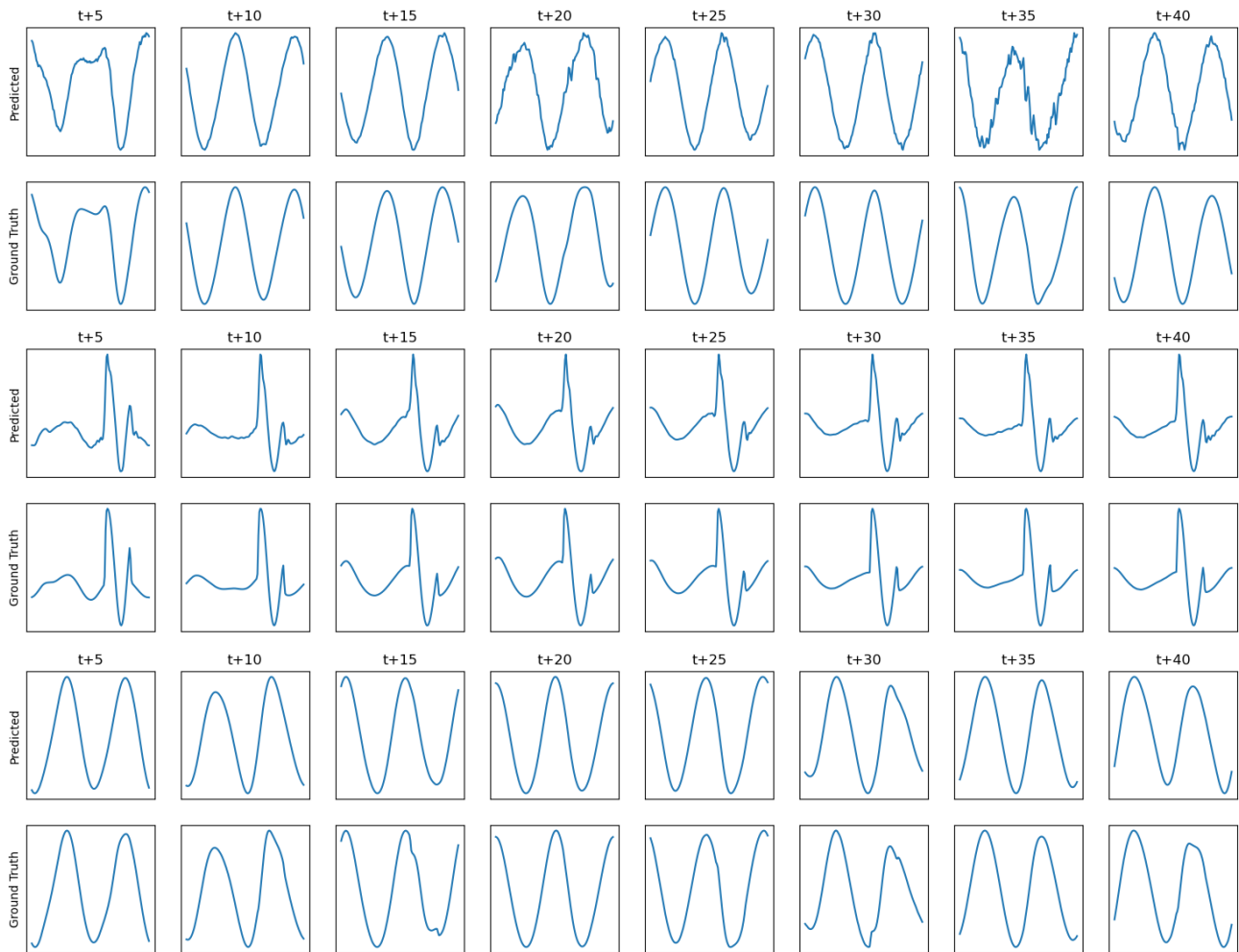




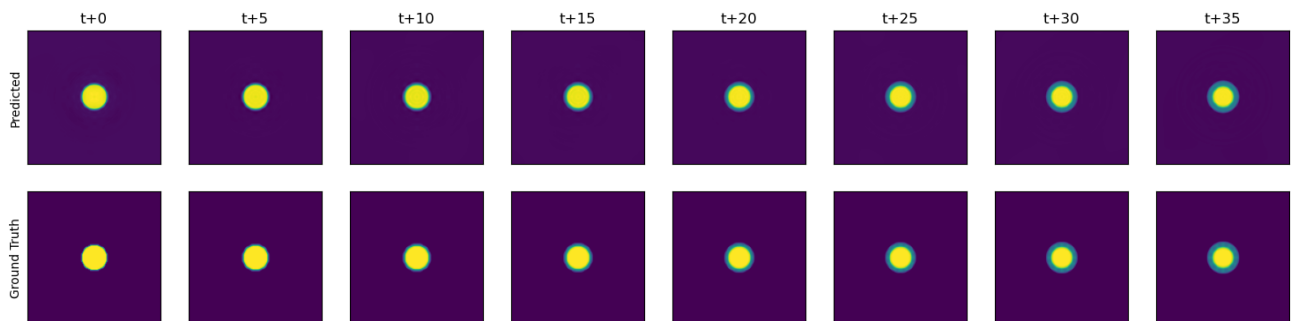
---

### D.3. 1D Navier Stokes

We show  $V_x$ , density, and pressure.



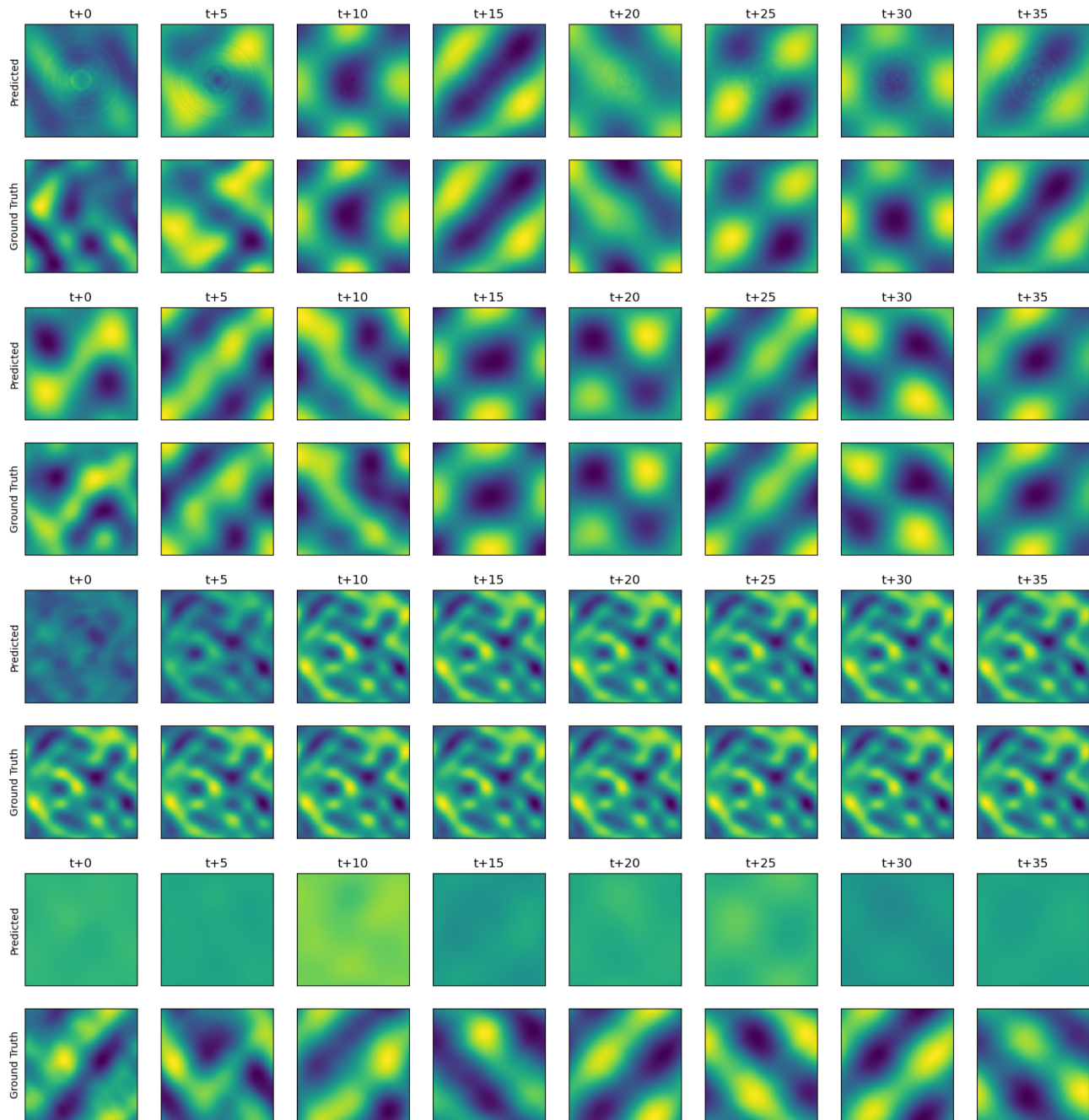
### D.4. Shallow Water



---

## D.5. 2D Navier Stokes

We show  $V_x$ ,  $V_y$ , density, and pressure.



In the prediction for 2D compressible Navier-Stokes we see a few artifacts in our generation. Furthermore, for quantities like pressure, our network often seems to generate an overly smoothed output. This could be because the 2D Navier-Stokes is the only PDE in our dataset that requires us to model pressure, and therefore the network is biased towards predicting a uniform value, which in our case is 0. We believe this can be avoided by adding more families of PDEs that model pressure, and is a fertile ground for future work.